Colloids and Surfaces B: Biointerfaces 173 (2019) 571–580

Contents lists available at ScienceDirect

Colloids and Surfaces B: Biointerfaces

journal homepage: www.elsevier.com/locate/colsurfb

Quantifying the interactions between biomimetic biomaterials – collagen I, collagen IV, laminin 521 and cellulose nanofibrils – by colloidal probe microscopy

Robertus Wahyu N. Nugroho[a], Riina Harjumäki[a,b], Xue Zhang[a], Yan-Ru Lou[b], Marjo Yliperttula[b,c], Juan José Valle-Delgado[a,*], Monika Österberg[a,*]

[a] Department of Bioproducts and Biosystems, School of Chemical Engineering, Aalto University, FI-00076 Aalto, Finland
[b] Division of Pharmaceutical Biosciences, Faculty of Pharmacy, University of Helsinki, FI-00014 Helsinki, Finland
[c] Department of Pharmaceutical and Pharmacological Sciences, University of Padova, I-35131 Padova, Italy

ARTICLE INFO

Keywords:
Collagen
Laminin
Cellulose nanofibrils
Surface forces
Adhesion
AFM-colloidal probe technique

ABSTRACT

Biomaterials of different nature have been and are widely studied for various biomedical applications. In many cases, biomaterial assemblies are designed to mimic biological systems. Although biomaterials have been thoroughly characterized in many aspects, not much quantitative information on the molecular level interactions between different biomaterials is available. That information is very important, on the one hand, to understand the properties of biological systems and, on the other hand, to develop new composite biomaterials for special applications. This work presents a systematic, quantitative analysis of self- and cross-interactions between films of collagen I (Col I), collagen IV (Col IV), laminin (LN-521), and cellulose nanofibrils (CNF), that is, biomaterials of different nature and structure that either exist in biological systems (e.g., extracellular matrices) or have shown potential for 3D cell culture and tissue engineering. Direct surface forces and adhesion between biomaterials-coated spherical microparticles and flat substrates were measured in phosphate-buffered saline using an atomic force microscope and the colloidal probe technique. Different methods (Langmuir-Schaefer deposition, spin-coating, or adsorption) were applied to completely coat the flat substrates and the spherical microparticles with homogeneous biomaterial films. The adhesion between biomaterials films increased with the time that the films were kept in contact. The strongest adhesion was observed between Col IV films, and between Col IV and LN-521 films after 30 s contact time. In contrast, low adhesion was measured between CNF films, as well as between CNF and LN-521 films. Nevertheless, a good adhesion between CNF and collagen films (especially Col I) was observed. These results increase our understanding of the structure of biological systems and can support the design of new matrices or scaffolds where different biomaterials are combined for diverse biological or medical applications.

1. Introduction

Materials for different biomedical applications have been extensively investigated for the last decades. [1–11] In many cases, the studies have been focused on the response of living cells to different materials, which has an impact on, for instance, the design of implants and scaffolds for tissue replacement or regeneration, and the development of materials for 2D and 3D cell cultures [12–22]. Materials of biological origin have gained a special interest in cell and tissue engineering because of their biocompatibility and non-toxicity, among other characteristics. Proteins like collagen, laminin, fibrin or fibronectin, and polysaccharides like agarose, alginate, hyaluronic acid, chitosan or cellulose are examples of biomaterials of interest for these applications. Although there is a considerable effort to understand cell-biomaterial interactions [23], not much attention has been paid to analyze biomaterial-biomaterial interactions [24], in spite that such interactions occur frequently in nature and in human tissues. A deeper insight into biomaterial-biomaterial interactions could provide a better understanding of the behavior of biological systems and could support the development of materials to mimic them.

Collagens are one of the main components of the extracellular matrix (ECM), an intricate network of assembled molecules that surrounds cells in tissues. [25] The ECM provides structural support and specific signaling pathways to cells, and regulates cell adhesion, migration and

* Corresponding authors.
E-mail addresses: juanjose.valledelgado@aalto.fi (J.J. Valle-Delgado), monika.osterberg@aalto.fi (M. Österberg).

https://doi.org/10.1016/j.colsurfb.2018.09.073
Received 4 July 2018; Received in revised form 12 September 2018; Accepted 28 September 2018
Available online 29 September 2018
0927-7765/ © 2018 The Authors. Published by Elsevier B.V. This is an open access article under the CC BY license (http://creativecommons.org/licenses/BY/4.0/).

differentiation [26]. The most abundant collagen in the human body, type I collagen (Col I), has a fibrillar morphology. Col I microfibrils of about 4 nm in diameter and an axial periodicity of 67 nm are formed by tropocollagen monomers that show a characteristic triple-helix structure. Collagen-collagen and collagen-proteoglycans interactions determine the interfibrillar spacing and the structure of the ECM, which is important, for example, for corneal transparency [27]. Collagen microfibrils can self-assemble into larger collagen fibers in connective tissues like tendon, cartilage, and skin [28]. The tensile stiffness and resilience of those tissues are also mainly due to collagen-proteoglycans and collagen-collagen (interfibril and interfiber) interactions. Laminin is another protein present in the ECM that plays an important role in cell adhesion. Collagen-laminin interactions are expected to be essential for the cell support function of ECM, but not much is yet known about these forces.

Basement membrane separates connective tissues from endothelia, epithelia, nervous system, and muscle fibers. Together with laminin and proteoglycans, type IV collagen (Col IV) is present in the basement membrane in the form of net-like structures. [29] Col IV and laminin play an essential role in the basement membrane formation and stability via self-interactions and interactions with other components [30]. Bruch's membrane, which provides structural support for retinal pigment epithelial (RPE) cells in eyes, is another example of biomaterial-biomaterial association. Bruch's membrane consists of 5 layers alternating Col IV and Col I, in addition to other molecules [31,32]. For instance, Col IV is present in the outermost layer, the basement membrane of the RPE, together with laminin, fibronectin, heparan sulfate and chondroitin/dermatan sulfate. The next layer, the inner collagenous layer, contains Col I besides Col III, Col V, hyaluronic acid and chondroitin/dermatan sulfate. The collagen stratification was mimicked in a recent work to grow human embryonic stem cell derived retinal pigment epithelial (hESC-RPE) cells *in vitro* [33]. Two-layer, Col IV over Col I films successfully support hESC-RPE growth, maturation and functionality *in vitro*. Nevertheless, Col I-Col IV interaction has not been studied in detail yet.

Due to its biocompatibility and excellent mechanical properties, plant-derived cellulose nanofibrils (CNF, also called nanofibrillated cellulose, NFC) have been introduced in 3D scaffolds for tissue engineering. [34,35] Formed by the self-assembly of linear molecules of cellulose, CNF are typically 5–60 nm in diameter and up to several micrometers in length [36]. CNF hydrogels successfully promote 3D growth and differentiation of human hepatic cells and human pluripotent stem cells [37–39]. Future applications of CNF in tissue engineering may still require the combination of CNF with ECM proteins –collagen and laminin– in a new generation of scaffolds to enhance cell adsorption. A quantitative characterization of the CNF-protein adhesion forces would be extremely valuable for the design of those scaffolds, as well as for better understanding the interactions of CNF implants with surrounding biological tissues.

The atomic force microscope (AFM) is a versatile instrument that combines subnanometric spacial resolution and high sensitivity (~ 10 pN) at force detection. Furthermore, it can operate in liquid environments. All these features make the AFM a very powerful tool for the characterization of biological samples at micro/nano-scale. [40] The colloidal probe technique (also known as colloidal probe microscopy) is a common AFM approach for the direct measurement of the surface forces between a spherical microparticle –attached at the end of an AFM cantilever– and a substrate [41,42]. Compared to sharp AFM tips (where the tip radius is usually not accurately known), the use of spherical microparticles in AFM force measurements offers a better control of the geometry of the interacting surfaces. The AFM-colloidal probe technique has been successfully applied to study the interactions between different materials, including cellulose surfaces [43–46]. However, force experiments to unravel the interaction forces between biomaterials composing biological systems or engineered tissues are almost non-existent.

Using the AFM-colloidal probe technique, we have quantified for the first time, to the best of our knowledge, the interaction forces and adhesion between Col I, Col IV, laminin-521, and CNF, *i.e.*, biomaterials of different nature (protein or polysaccharide) and morphology (fibrillar or non-fibrillar structure) that are either key components of biological systems or promising materials for tissue engineering applications.

2. Materials and methods

2.1. Preparation of collagen and laminin solutions, and CNF dispersions

Solutions of Col I and Col IV from human placenta (Sigma-Aldrich, St. Louis, MO, catalog numbers C7774 and C7521, respectively) were prepared similarly as described by Goffin et al. [47] Briefly, both collagens were initially dissolved to 1 mg/ml concentration at 4 °C in diluted acetic acid, pH 3. Collagen solution aliquots were subsequently stored at −20 °C. Prior to use, collagen solutions were thawed by sonication in a water bath with ice for two periods of 10 min with 10 min rest period in between.

Human recombinant laminin-521 (LN-521) 10 mg/ml solution (BioLamina, Sundbyberg, Sweden) was diluted in Dulbecco's phosphate-buffered saline supplied with calcium and magnesium salts (DPBS+, Gibco™) to a final concentration of 10 µg/ml following the manufacturer's instructions.

CNF dispersions were prepared from CNF hydrogel (Growdex®, UPM Biochemicals, Helsinki, Finland), 0.875% dry matter content, following the protocol described by Valle-Delgado et al. [48] Briefly, CNF hydrogel was diluted in Milli-Q water and ultrasonicated at 25% amplitude for 5 min with a Branson sonifier S-450 D (Branson Corp., Danbury, CT). The dispersion was subsequently centrifuged at 8000 × *g* for 30 min at room temperature using an Eppendorf centrifuge 5804R (Eppendorf, AG, Hamburg, Germany) to separate CNF fibrils from larger aggregates. The supernatant fraction containing CNF fibrils was collected and utilized to prepare CNF films and coatings.

2.2. Preparation of biomaterial films

Biomaterial films were prepared on flat substrates using different deposition techniques. Collagen films were obtained applying the Langmuir-Schaefer (LS) method as described by Sorkio et al. [33] using a KSV minitrough system (KSV Instruments, Helsinki, Finland). Briefly, sonicated collagen solution was randomly spread on subphase consisting of 2 × phosphate-buffered saline (PBS). The system was allowed to equilibrate for 30 min to achieve a homogeneous distribution of collagen molecules at the air-buffer interface. The collagen films were compressed to 12 N/m and 30 N/m deposition pressures for Col I and Col IV, respectively, at 65 mm/min compression rate. They were then deposited onto freshly cleaved mica substrates and dried overnight in a desiccator. The films were subsequently rinsed with MilliQ water to remove salt crystals, dried, and stored at room temperature before use.

LN-521 films were prepared by adsorption, following a protocol provided by the supplier. Plastic cover slips (Sarstedt, Nümbrecht, Germany) were covered with 10 µg/ml LN-521 solution in 1 x DPBS + for two hours at room temperature. After adsorption, the LN-521 films were kept in 1 x DPBS+ at 4 °C and used within 3 weeks. LN-521 films were also rinsed with Milli-Q water and dried for topographical imaging.

CNF films were obtained by spin-coating CNF dispersions on mica substrates previously coated with polyethylene imine (PEI) to enhance CNF adsorption, as described elsewhere. [48] The spin-coating was carried out at 4000 rpm for 1 min using a Laurell spin-coater WS-650SX-6NPP-Lite (Laurell Technologies Corp., North Wales, PA).

2.3. Preparation of colloidal probes

Tipless silicon cantilevers CSC38/No Al (MikroMasch, Wetzlar, Germany), with normal spring constants in the range 0.01-0.36 N/m, were used to measure biomaterial-biomaterial interactions. The spring constants were determined via the analysis of thermal vibration spectra and the application of Sader's equation. [49] Colloidal probes were prepared by attaching glass microspheres of 15–45 μm diameter (Polysciences, Inc., Warrington, PA) at the free end of the cantilevers using a motorized PatchStar micromanipulator (Scientifica, Uckfield, UK) and an optical adhesive (Norland Products, Inc., Cranbury, NJ) cured under UV light.

The colloidal probes (microspheres attached to cantilevers) were coated with Col I, Col IV, LN-521, and CNF following different procedures. In order to get collagen-coated colloidal probes, the glass microspheres were cleaned with piranha solution for 15 min, rinsed with Milli-Q water, and coated with (3-aminopropyl) triethoxysilane (APTES) before being attached to the cantilevers. The coating of the glass microspheres with APTES aimed at enhancing the subsequent adsorption of collagen, and took place by immersing the microspheres in 5% (v/v) APTES solution in ethanol for 45 min at room temperature followed by thorough rinsing with ethanol several times and overnight drying. Colloidal probes made with APTES-coated glass microspheres were mounted on metallic discs with double-sided tape and a few drops of collagen solutions were then spin-coated on the probes at 1000 rpm for 40 s. The collagen-coated probes were dried overnight and rinsed with Milli-Q water before use.

Laminin-coated colloidal probes were prepared just before the force measurements by immersing the pre-mounted colloidal probes in drops of 10 μg/ml LN-521 solution in 1 x DPBS+ for two hours at room temperature. Laminin-coated probes were rinsed by dipping in 1 x DPBS+ drops before the force measurements, always preventing the laminin from getting dry.

CNF-coated probes were also prepared by dip-coating. Firstly, the pre-mounted colloidal probes were dipped in drops of 2.5 mg/ml PEI solution for 10 min and rinsed by dipping in Milli-Q water. Then the PEI-coated colloidal probes were immersed in drops of CNF dispersions for 10 min, rinsed by dipping in Milli-Q water and finally dried under flowing nitrogen.

2.4. Atomic force microscopy

A MultiMode 8 AFM with NanoScope V controller and an E scanner (Bruker, Billerica, MA) was utilized to obtain high-resolution images of the biomaterial films and coatings. Two scanning operation modes were used: tapping mode with NCHV-A probes (Bruker AFM Probes, Camarillo, CA) for imaging flat films, and ScanAsyst mode with ScanAsyst-air probes (Bruker AFM Probes) for imaging coated colloidal probes. The samples were scanned in air. Research NanoScope 8.15 or NanoScope Analysis 1.5 softwares (Bruker) were used for image analysis. The only image correction applied was flattening.

2.5. Force measurements by AFM-colloidal probe technique

Biomaterial-biomaterial force measurements were conducted in 1 x PBS using a MultiMode 8 AFM with NanoScope V controller coupled with a Pico Force scanner (Bruker). A biomaterial-coated flat substrate and a biomaterial-coated colloidal probe were mounted in the liquid cell of the AFM, and the system was allowed to equilibrate for 10 min in 1 x PBS at room temperature. The surface forces between the biomaterial films were measured while approaching the flat substrate and the colloidal probe until contact and during the subsequent retraction. The approach-retraction cycle was performed at a typical rate of 2 μm/s. The surfaces were kept in contact for different times (1 s, 10 s, and 30 s) before retracting them. For each system, between 20 and 120 force curves were collected at each contact time with the same or different probes on at least three random locations of the same or different flat films to check data reproducibility. The raw interaction data were transformed into force-*versus*-separation curves using the AFM Force IT software (ForceIT, Sweden). Briefly, the force values were obtained by multiplying the photodector signal by the spring constant of the cantilevers and the deflection sensitivity of the setup (the latter obtained from force curves on a hard surface, like freshly cleaved mica or silica); the probe-substrate separation distance was calculated as the scanner position plus the cantilever deflection (Figure S1, supplementary data) [42,50]. Zero interaction force was assigned to the curve baseline, whereas zero separation was assumed at the position of maximum applied force. The force curves were normalized by the radius of the colloidal probe. The approach force curves were compared to the prediction from the classical DLVO theory, [51–53] using a Hamaker constant of 7.5×10^{-21} J for proteins and 8.0×10^{-21} J for cellulose [54,55]. Biomaterial-biomaterial adhesion energies were calculated by integrating the areas enclosed between the retraction force curves and the zero baselines. Control experiments between bare glass colloidal probes and biomaterial films deposited on flat substrates were also carried out.

2.6. Statistical analysis

Mean values of root mean square (RMS) surface roughness of biomaterial films were calculated from 2 to 3 AFM images of 1×1 μm^2 area, and the corresponding standard deviations were used as errors. The adhesion energies for biomaterial-biomaterial interactions were also presented as mean values ± standard deviations, which were obtained from the analysis of n force curves ($20 < n < 120$). Welch's t-test was used to ascertain whether the mean values of two independent groups of adhesion energy data were significantly different ($p \leq 0.05$). All the statistical analyses were carried out with OriginPro software (OriginLab Corporation, Northampton, MA).

3. Results and discussion

3.1. Topographical characterization of biomaterial films deposited on flat substrates

Different deposition techniques –LS, spin-coating, or simply adsorption– were applied in order to get homogeneous model films of biomaterials on flat substrates. AFM topography images of the films are shown in Fig. 1a–d, with corresponding cross-section profiles in Fig. 1e–h. The presence of hydrophobic domains in collagen molecules favours their spreading at the PBS-air interface, facilitating the application of LS method for collagen deposition on a mica substrate as previously demonstrated by Sorkio et al. [33] Before deposition, the Col I and Col IV films at the PBS-air interface were compressed to surface pressures of 12 mN/m and 30 mN/m, respectively, without provoking film collapse (Figure S2). Col I films obtained by LS deposition method consisted of Col I fibrils homogeneously distributed on the mica surface (Fig. 1a). Col IV films were meshworks of fine fibrils, sometimes associated into larger fibril bundles (Fig. 1b), resulting in rougher topography than Col I films (Table 1). Thicknesses of 7–11 nm and 31 nm have previously been reported for Col I and Col IV films, respectively, prepared by LS technique. [33]

Laminin films were obtained by adsorption on flat plastic cover slips. This procedure yielded homogeneous and smooth laminin films (Fig. 1c and Table 1), and ensured that the films were always in wet state, which is crucial for laminin to keep its adhesive properties. The laminin films were about 20 nm thick (Figure S3) and seemed to have a mesh-like structure, in accordance with previous studies showing that laminin can form networks by polymerization through terminal domains. [56–58]

CNF films were obtained by spin-coating CNF on top of PEI-covered mica substrates, following a well-established protocol. [48] Thicknesses

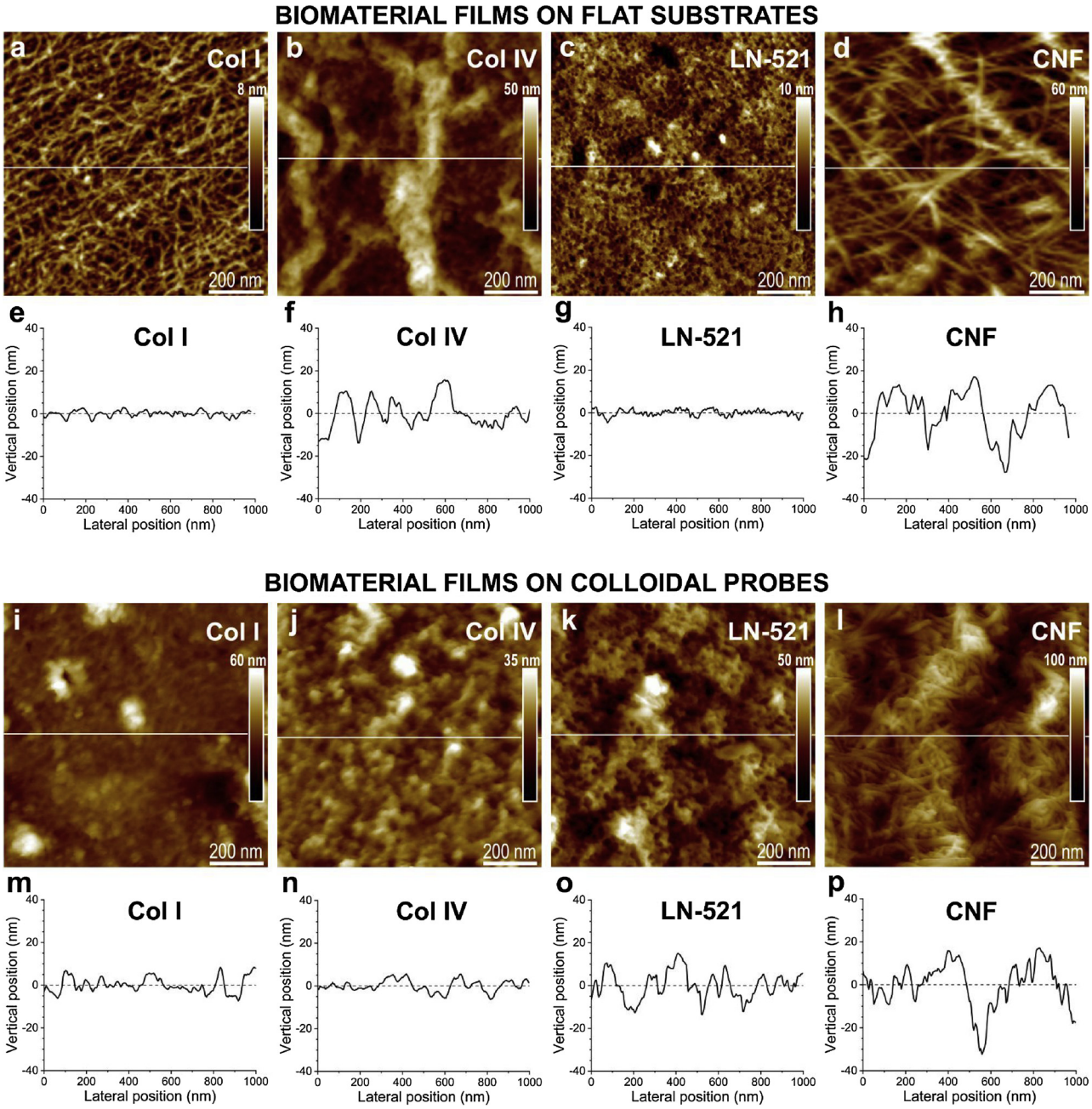

Fig. 1. AFM height images and cross-section profiles of different biomaterial films on flat substrates (a–h) and on spherical colloidal probes (i–p). The cross-section profiles corresponding to the white lines in (a–d) and (i–l) are presented in (e–h) and (m–p), respectively.

Table 1
Root mean square (RMS) surface roughness of different biomaterial films (mean values ± standard deviations).

Sample	RMS surface roughness (nm)	
	Colloidal probe	Flat substrate
Col I film	6.2 ± 0.7	1.9 ± 0.9
Col IV film	5.3 ± 1.5	7.69 ± 0.15
LN-521 film	7.2 ± 1.1	3.22 ± 0.02
CNF film	17.7 ± 1.5	10.9 ± 0.6
Bare glass microparticle	9.5 ± 2.4	–
Bare plastic cover slip	–	1.1 ± 0.4

of up to 8 nm were previously reported for spin-coated CNF films in dry state [45,59]. Fig. 1d shows a high-resolution AFM image of a typical CNF film, formed by intertwined cellulose fibrils of few nanometers in width and up to several micrometers in length. The CNF films were the roughest of the studied films, significantly rougher than the Col I and LN-521 films (Table 1).

3.2. Topographical characterization of biomaterial films deposited on microspherical probes

The coating of spherical glass microparticles with different biomaterials was a crucial aspect for the reliability of the measurements of biomaterial-biomaterial interactions using those microparticles as colloidal probes. Therefore, a special effort was made to develop successful methods to coat glass microparticles attached at the end of AFM

cantilevers with homogeneous and stable films of the selected biomaterials. A combined stepwise process involving microparticle surface chemistry modification with APTES and spin-coating of collagen was revealed to be more effective for the formation of homogeneous films of Col I fibrils and Col IV meshwork on the colloidal probes than the simply dip-coating in collagen solutions required by the LS method. The hydrophobization of the glass microparticles with APTES enhanced the adsorption of collagen molecules, which homogeneously spread on the particle surface during the spin-coating. Fig. 1i and j show high-resolution AFM images of glass probes coated with Col I and Col IV, respectively, and Fig. 1m and n present the corresponding cross-section profiles. Similarly to collagen films on flat substrates, Col I fibrils could be distinguished on Col I-coated probes (Fig. 1i), and a meshwork of fine fibrils could be observed on Col IV-coated probes (Fig. 1j). Unlike flat films (Fig. 1b), no Col IV association into larger fibril bundles were observed on Col IV-coated probes, suggesting that the spin-coating procedure could yield smoother Col IV films than the LS method used for flat films. The larger fiber-like bundles observed in LS films were probably formed during the compression of the Col IV films at the PBS-air interface. [33]

LN-521 and CNF were adsorbed on glass probes following similar procedures as for flat films. AFM analysis showed that the spherical probes were fully covered by laminin and CNF (Fig. 1k and 1l, respectively; cross-section profiles in Fig. 1o and p, respectively), with film structures similar as for flat substrates (Fig. 1c and d). LN-521 molecules adsorbed on the glass microparticles forming a mesh-like arrangement, whereas intertwined nanofibrils of cellulose were clearly observed on CNF-coated probes. Compared to flat substrates, the higher roughness of the glass microparticles affected the roughness of the biomaterial films adsorbed on them (Figure S3 and Table 1). Nevertheless, it should be noted that, with the exception of CNF, all the biomaterial coatings smoothed down the roughness of the bare glass probes. The stiffness and longer length of the nanofibrils of cellulose could affect the way CNF adsorbs on the curved surface of the glass microparticles, rendering CNF-coated probes significantly rougher than other biomaterial-coated probes.

The biomaterial films were still observed in AFM images of the colloidal probes after performing the force experiments, which confirmed the stability of the coatings. The reproducibility of the force curves provided further evidence of the stability of the biomaterial films during the force experiments.

3.3. Biomaterials self-interactions

The structural integrity of ECM and scaffolds for tissue engineering critically depends on biomaterial cohesion forces. Thus, the measurement of biomaterials self-interactions provides very relevant information for the characterization of biological and biomedical assemblies. Therefore, the AFM-colloidal probe technique was used in this work to measure the interaction forces between biomaterials films prepared on spherical probes and on flat substrates. In a typical experiment, the colloidal probe and the flat substrate were approached each other until contact, kept in contact for some time (1 s, 10 s, or 30 s), and finally retracted. All the force experiments were carried out in 1 x PBS at room temperature. Retraction force curves between colloidal probes and substrates coated with the same biomaterials are presented in Fig. 2 for different contact times (see the corresponding approach force curves in Figure S4). Force curves obtained at four different positions of the flat substrate are shown to indicate the reproducibility of the measurements. A considerable adhesion (that is, negative force values) was observed when retracting Col I films from contact (Fig. 2a). That adhesion increased with the contact time between the films, an effect especially evident for Col IV and LN-521 films (see Fig. 2b,c for retraction force curves and S5 for calculated adhesion energy). Increasing the contact time favoured the binding between molecules from opposing films, mainly via hydrogen bonds, van der Waals forces, and, in the case of protein films, also electrostatic attraction between oppositely charged groups. It has been reported that Col IV can self-associate via terminal domains (C-terminal NC1 and N-terminal 7S domains) and binding sites along the molecule length. [60,61] The higher tendency of Col IV molecules for self-assembly could explain why the adhesion observed between Col IV films was much stronger than between Col I films after 30 s contact time. Similarly, the ability of laminin to self-assemble through its N-terminal domains [56–58] leads to the formation of bonds between laminin molecules from opposing films during contact, resulting in stronger adhesion between the films as the contact time increased. In contrast to the protein films, a weak adhesion was observed between CNF surfaces that slightly increased with the contact time (Fig. 2d and S5). Van der Waals forces and a low number of hydrogen bonds are probably responsible of the low adhesion measured between CNF films.

A purely repulsive force was observed upon approach for all the studied biomaterials (Figure S4). A comparison of representative approach force curves for the different systems is presented in Fig. 3a. The repulsion observed at distances below 100 nm was clearly different from the predictions of the DLVO theory, indicating that the repulsion was not due to electrostatic double layer forces –mainly screened at the high ionic strength of 1 x PBS–, but due to the compression of the films. Thus, the zero separation in the graphs actually corresponds to the point of maximum compression of the films in our experiments (see Figure S1 for more details on converting raw data to normalized force-*versus*-separation curves; note that the AFM can not measure directly the separation distance between probe and substrate). Qualitatively, Fig. 3a shows that Col IV films could be compressed more than Col I and LN-521 films. This correlates with the morphology of the films observed in Fig. 1: while LN-521 and Col I films were smooth and probably more compact (Fig. 1a,c), Col IV formed a rougher film with fiber-like bundles that were probably more compressible (Fig. 1b). Compared to Col IV, the lower compression of CNF films could be associated to the higher stiffness of the nanofibrils of cellulose. It must be noted that the range and magnitude of the repulsion for each biomaterial were independent of the number of force measurements at the same or different spots, and were not affected by the time the films were kept in contact (Figure S4), suggesting that the materials quickly recovered from the induced deformation in between measurements. In agreement with our observations, Graham et al. found that Col I monomers recovered their conformation upon stretching within 1–5 s, [62] which was similar to the time scale of our force experiments.

Some representative retraction force curves for the different films after 30 s contact time are plotted together for a clearer comparison in Fig. 3b. Note that while the highest pull-off force was measured between LN-521 films, the longest range of adhesion occurred between Col IV films. Histogram analyses of the adhesion energy (calculated as the area enclosed between the retraction force curves and the zero baselines) at different contact times are presented in Fig. 3c–f. The histograms clearly show that the adhesion energy increased as the contact time between the films increased. Mean values of adhesion energy between the different films after 30 s contact time are compared in Fig. 3g. They were all significantly different from each other ($p \leq 0.05$). The adhesion energies between Col IV films (1.42 ± 0.19 nJ/m) and between LN-521 films (0.67 ± 0.10 nJ/m) were significantly higher than between Col I films (0.18 ± 0.03 nJ/m), whereas a very low adhesion energy was measured between CNF films (0.028 ± 0.015 nJ/m). Similar trends were observed for the adhesion energies after 1 s contact time, except that no significant difference between Col I and Col IV was detected in that case (Figure S5). In fact, the formation of the strong bonds that differentiate the adhesion of Col IV from Col I films required contact times larger than 10 s (Figure S5), suggesting that sustained compression of the films favours the accessibility of crosslinking domains in Col IV molecules.

Control experiments between bare colloidal probes and biomaterials films revealed a very weak adhesion between uncoated glass-

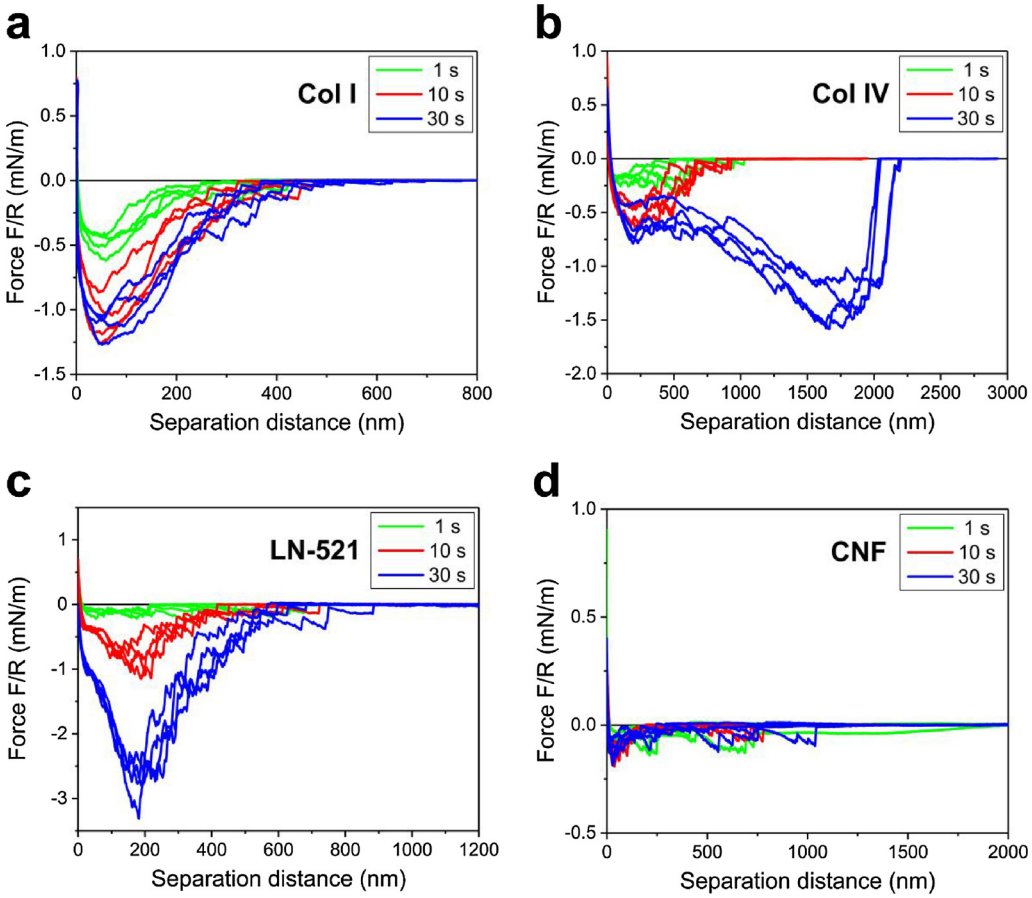

Fig. 2. Retraction force curves between (a) Col I films, (b) Col IV films, (c) LN-521 films, and (d) CNF films measured at four different locations and different contact times. Force values were normalized by the probe radius R (R = 11.2 µm, 10.3 µm, 8.2 µm, and 15.9 µm for Col I, Col IV, LN-521, and CNF, respectively).

microparticles and protein films (Figure S6), clearly different from biomaterial-biomaterial interactions. This observation, together with the AFM images, is a strong evidence of the successful coating of the probes and the stability of those coatings during biomaterial-biomaterial force measurements.

Vidal et al. have reported pull-off forces in the range 50–500 pN between Col I fibrils adsorbed on gold substrates and AFM tips after 2 s contact time in PBS, values that significantly increased in the presence of different crosslinking agents. [24] In contrast, pull-off forces in the range 5–7 nN were obtained in our experiments between Col I films after 1 s contact time (Fig. 2a). The apparent discrepancy of these results could be explained from the different set-up of the experiments: while Vidal et al. used Col I-coated sharp AFM tips, Col I-coated microspherical probes were used in this work which increased the contact area and, consequently, the adhesion between the Col I films. Furthermore, the AFM images point out that the Col I coating density of the substrates seemed to be higher in our case.

It is also interesting to mention that, by pulling Col I fibrils or type I tropocollagen molecules using AFM-force spectroscopy, Graham et al. and Bozec and Horton observed that forces between hundreds of pN and few nN were needed to stretch Col I monomers. [62,63] A similar range of forces were measured in our experiments (Fig. 2), indicating that the irregular jumps observed in the retraction force curves corresponded to the stretching and rupture of bound Col I molecules, the number of which increased with the time in contact between the films.

3.4. Cross-interactions between Col I, Col IV and LN-521

Besides the characterization of biomaterials self-interactions, one of the main objectives of this work is to unravel the cross-interactions between different protein components of ECM and basement membranes. The quantification of those interactions is basically unexplored in spite of the high interest to understand and mimic biological systems for tissue engineering applications. Cross-interactions between Col I, Col IV, and LN-521 films were measured by AFM-colloidal probe technique in the same way as explained before for self-interactions. A/B is the notation used henceforth to describe the cross-interaction between a colloidal probe coated with biomaterial A and a flat substrate coated with biomaterial B. Approach and retraction force curves for the cross-interaction between Col I, Col IV, and LN-521 films are presented in Fig. 4 and S7.

Similarly to biomaterial self-interactions, a non-DLVO repulsion was observed in the approach force curves due to the compression of the films (Fig. 4a and S7). The retraction force curves, on the other hand, showed different adhesion intensities for the cross-interactions of different films (Fig. 4b). The cross-adhesion between protein films became significantly stronger as the contact time increased, as can be observed in Fig. 4c–f and in the histogram analyses of adhesion energy presented in Figure S8.

3.4.1. Col I-Col IV cross-interactions

For comparison, the cross-interaction between Col I and Col IV was studied in both Col I/Col IV and Col IV/Col I configurations. Adhesion energies of 0.55 ± 0.07 nJ/m and 0.30 ± 0.03 nJ/m were obtained for Col I/Col IV and Col IV/Col I, respectively, after 30 s contact time (Fig. 5a). The difference between the adhesion energies of Col I/Col IV and Col IV/Col I could be due to different structure of Col IV films deposited by LS and spin-coating methods. Indeed, Col IV association into larger fiber-like bundles were observed on LS films deposited on flat mica substrates (Fig. 1b), but smoother Col IV films without those

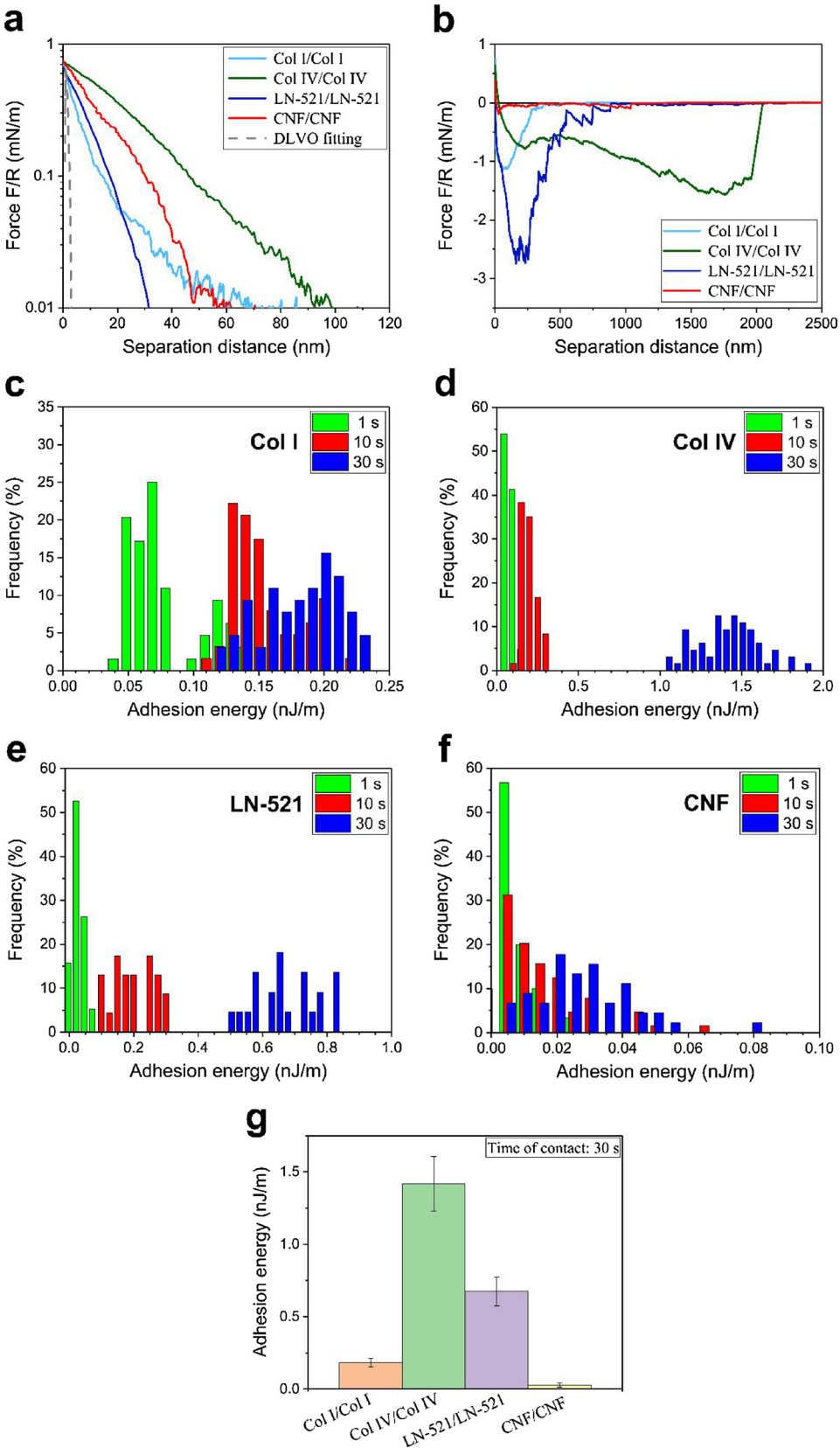

Fig. 3. Self-interaction and adhesion energy between biomaterial films. (a,b) Representative approach (a) and retraction (b) force curves for 30 s contact time. (c–f) Histogram analyses of the adhesion energy between Col I (c), Col IV (d), LN-521 (e), and CNF (f) films after different contact times. (g) Adhesion energy between different films after 30 s contact time. Force and adhesion energy values were normalized by the probe radius R (see caption of Fig. 2). The dashed line in (a) corresponds to DLVO prediction for 150 mM ionic strength (PBS). Mean values and standard deviations ($20 < n < 80$) are presented in (g). Mean values in (g) are all significantly different from each other according to Welch's t-test ($p \leq 0.05$).

aggregates were obtained by spin-coating on spherical colloidal probes (Fig. 1j). The structure of Col IV LS films made them more easily compressible (Fig. 4a), which could increase the number of crosslinking points between the collagen films and, consequently, the adhesion in Col I/Col IV force experiments.

3.4.2. Collagen-laminin cross-interactions

The strongest adhesion was observed between Col IV and LN-521 films (Figs. 4b and 5 a). The adhesion energy between Col IV and LN-521 after 30 s contact time was 1.9 ± 1.0 nJ/m, significantly higher than the self-adhesion energies of Col IV (1.42 ± 0.19 nJ/m) and LN-

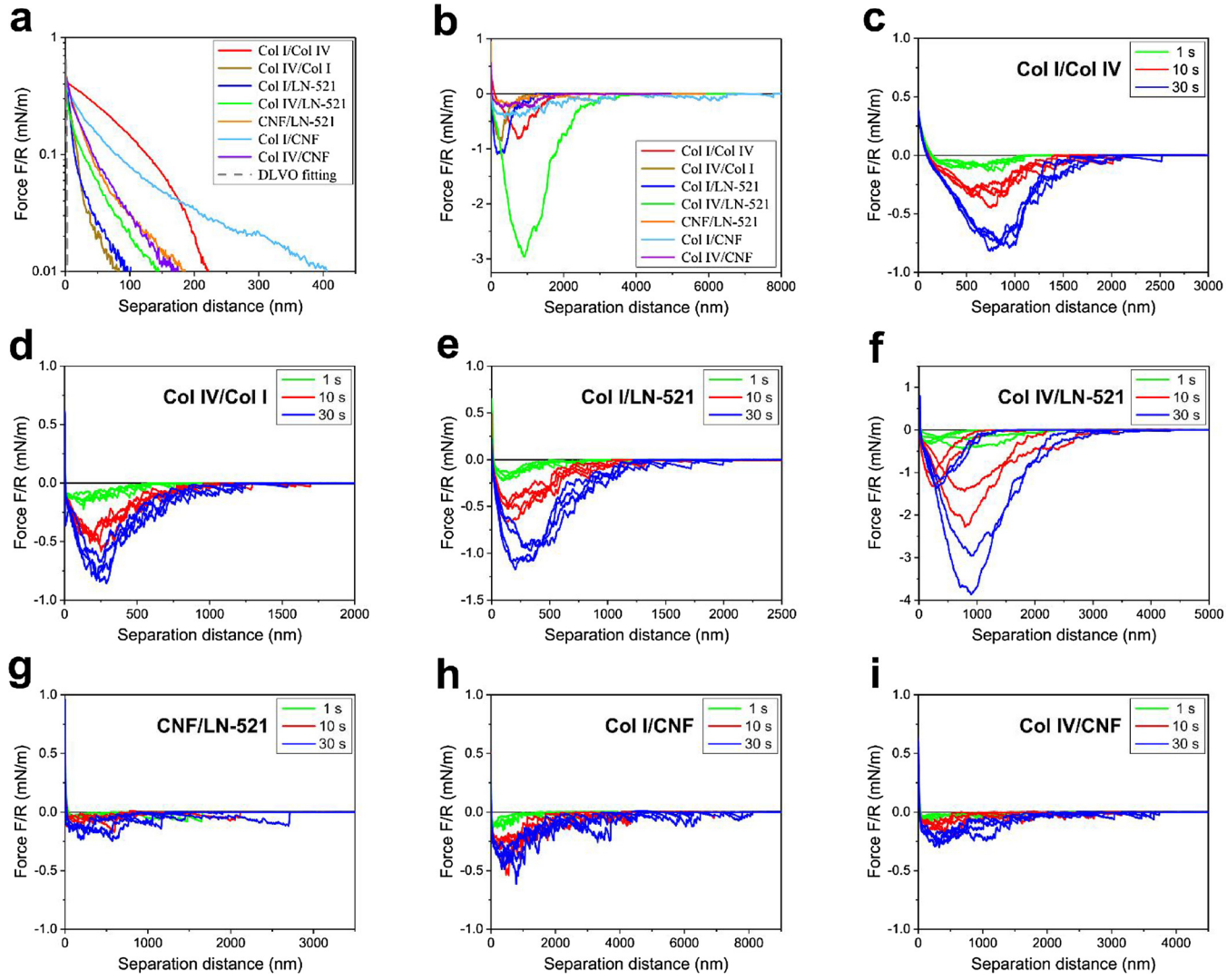

Fig. 4. Cross-interaction between different biomaterial films. (a,b) Representative approach (a) and retraction (b) force curves for 30 s contact time. (c–i) Retraction force curves for Col I/Col IV (c), Col IV/Col I (d), Col I/LN-521 (e), Col IV/LN-521 (f), CNF/LN-521 (g), Col I/CNF (h), and Col IV/CNF (i) measured at four different locations and different contact times. Force values were normalized by the probe radius R (R = 22.0 μm, 17.9 μm, 15.2–16.3 μm, 14.0–17.7 μm, 13.1 μm, 15.8 μm, and 16.7–17.9 μm for Col I/Col IV, Col IV/Col I, Col I/LN-521, Col IV/LN-521, CNF/LN-521, Col I/CNF, and Col IV/CNF, respectively). The dashed line in (a) corresponds to DLVO prediction for 150 mM ionic strength (PBS).

521 (0.67 ± 0.10 nJ/m). The strong adhesion between Col IV and LN-521 is mainly due to the ability of laminin to bind Col IV via the globular regions of either of its four arms. [64] That strong adhesion provides structural stability to basement membranes, of which Col IV and LN-521 are main components.

It has been reported that laminin binds preferentially to Col IV over other collagens. [65] Here we provide quantitative support to that observation: the adhesion energy of LN-521 to Col IV (1.9 ± 1.0 nJ/m)

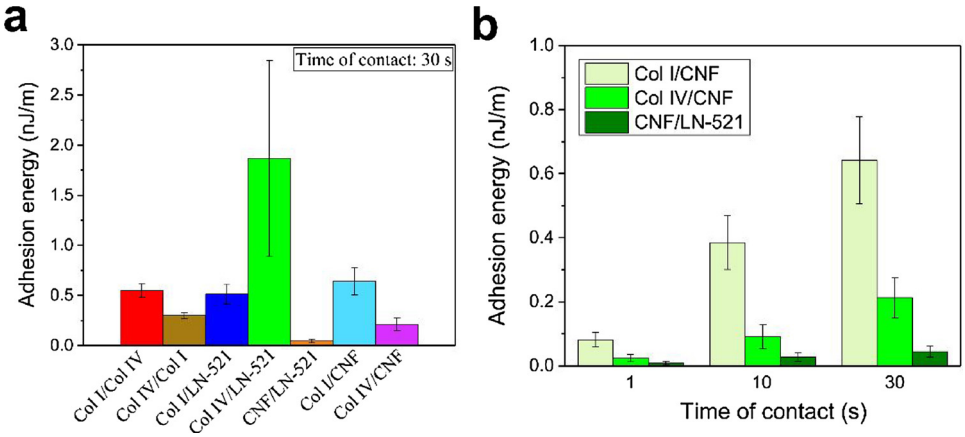

Fig. 5. Adhesion energy for the cross-interaction of different biomaterials. (a) Adhesion energy between different films after 30 s contact time. (b) Adhesion energy between CNF and protein films (Col I, Col IV, and LN-521) after different contact times. Adhesion energy values were normalized by the probe radius (see caption of Fig. 4). Mean values and standard deviations are presented ($35 < n < 120$). Mean values are all significantly different from each other according to Welch's t-test ($p \leq 0.05$).

was considerably higher than to Col I (0.51 ± 0.09 nJ/m, Fig. 5a and Figure S9). Nevertheless, the adhesion between LN-521 and Col I is still appreciable and reflects the strength of the binding of laminin to Col I fibrils in biological systems (ECM, for instance). It can also be observed that the energies of the adhesion of Col I to either Col IV or LN-521 are quite similar. These results provide a quantitative explanation for the structural integrity of the Bruch's membrane, formed by 5 layers alternating Col IV (with laminin) and Col I. The considerable adhesion between Col I and Col IV and between Col I and laminin provides strong connection between adjacent layers in the Bruch's membrane.

3.5. Cross-interactions of CNF with proteins

The potential application of CNF in tissue engineering is strongly supported by the successful utilization of CNF in 3D cell growth and differentiation. [37–39] Especially interesting in this research area is to understand how CNF interacts with other biomaterials involved in cell support and adhesion, for example, collagen and laminin in ECM. Thus, the cross-interaction of CNF with Col I, Col IV, and LN-521 has been quantified in this work by AFM-colloidal probe technique. The approach force curves between CNF and other biomaterials were qualitatively similar to the ones obtained for the cross-interaction of other biomaterials, showing a non-DLVO repulsion due to the compression of the films (Fig. 4a and S7). The adhesion observed in the retraction force curves (Fig. 4b,g–i) revealed that the affinity of CNF to Col I, Col IV, and LN-521 was different. The adhesion was contact time dependent, as can be seen in Fig. 5b. Among the protein biomaterials studied, CNF bound the strongest to Col I, with an adhesion energy of 0.64 ± 0.14 nJ/m after 30 s contact time. Although statistically different, that adhesion energy was in the same range as the values obtained between Col I and Col IV and between Col I and LN-521 (Fig. 5a). In spite of the different chemical nature of CNF –a polysaccharide made of glucose units– and the proteins Col IV and LN-521, Col I showed a similar binding affinity to all of them, most probably through van der Waals forces and hydrogen bonds. A moderate adhesion was observed between CNF and Col IV with an adhesion energy of 0.21 ± 0.06 nJ/m after 30 s contact time, significantly lower than between CNF and Col I. In contrast, a very low adhesion was detected between CNF and LN-521. The adhesion energy between CNF and LN-521 films was only 0.044 ± 0.018 nJ/m after 30 s contact time, not far in magnitude to the self-adhesion of CNF films. Since laminin favours the adhesion of cells to ECM, the incorporation of laminin into CNF matrices could have been a natural approach to develop new CNF-based scaffolds with enhanced cell adhesion properties. However, the low affinity observed between CNF and laminin indicates that the combination of CNF and laminin could not be a good strategy. Instead, collagen or a combination of collagen and laminin would guarantee a better adhesion of cells to CNF-based scaffolds.

4. Conclusions

Self- and cross-interactions between Col I, Col IV, LN-521, and CNF films in PBS were quantified using the AFM-colloidal probe technique. For that, different procedures were developed to coat microspherical glass probes with homogeneous films of each biomaterial. No attraction was detected when approaching the biomaterial-coated probes to flat biomaterial films obtained by Langmuir-Schaefer, spin-coating or adsorption methods; only a long-ranged repulsion was observed due to the compression of the films. On the other hand, the analysis of the retraction force curves showed that the adhesion between biomaterial films increased with the contact time. High adhesion energies were measured for self- and cross-interactions between Col IV and LN-521 films, results that are directly connected to the structural integrity of basement membranes. A considerable adhesion was also measured between LN-521 and Col I films, as well as between Col I and Col IV films, which explains the strong association of these materials in adjacent layers of Bruch's membrane or, in general, in ECM. In spite of its different polysaccharide nature, CNF adheres very well to Col IV and, especially, Col I films, but poor adhesion to LN-521 films was observed. These results are relevant for potential application of CNF in tissue engineering. In fact, besides providing a deeper quantitative understanding of the interactions between different biomaterials in biological systems, the results of this work can support the design of new matrices or scaffolds where different biomaterials could be combined for diverse biological or medical applications.

Data availability

The raw/processed data required to reproduce these findings cannot be shared at this time as the data also forms part of an ongoing study.

Declaration of interest

None.

Acknowledgements

This work was funded by the Academy of Finland (project number 278279, MIMEGEL). The CNF Growdex® used in this work was kindly supplied by UPM Biochemicals (Helsinki, Finland). The authors thank Elina Vuorimaa-Laukkanen for fruitful scientific discussions on collagen films preparation by LS.

Appendix A. Supplementary data

Supplementary material related to this article can be found, in the online version, at doi:https://doi.org/10.1016/j.colsurfb.2018.09.073.

References

[1] A. Vedadghavami, F. Minooei, M.H. Mohammadi, S. Khetani, A.R. Kolahchi, S. Mashayekhan, A. Sanati-Nezhad, Manufacturing of hydrogel biomaterials with controlled mechanical properties for tissue engineering applications, Acta Biomater. 62 (2017) 42–63.
[2] N.H.C.S. Silva, C. Vilela, I.M. Marrucho, C.S.R. Freire, C.P. Neto, A.J.D. Silvestre, Protein-based materials: from sources to innovative sustainable materials for biomedical applications, J. Mater. Chem. B 2 (2014) 3715–3740.
[3] T.H. Silva, A. Alves, B.M. Ferreira, J.M. Oliveira, L.L. Reys, R.J.F. Ferreira, R.A. Sousa, S.S. Silva, J.F. Mano, R.L. Reis, Materials of marine origin: a review on polymers and ceramics of biomedical interest, Int. Mater. Rev. 57 (2012) 276–306.
[4] K.L. Spiller, S.A. Maher, A.M. Lowman, Hydrogels for the repair of articular cartilage defects, Tissue Eng. Part B Rev. 17 (2011) 281–299.
[5] M. Navarro, A. Michiardi, O. Castaño, J.A. Planell, Biomaterials in orthopaedics, J. R. Soc. Interface 5 (2008) 1137–1158.
[6] C.P. Barnes, S.A. Sell, E.D. Boland, D.G. Simpson, G.L. Bowlin, Nanofiber technology: designing the next generation of tissue engineering scaffolds, Adv. Drug Deliv. Rev. 59 (2007) 1413–1433.
[7] M. Martina, D.W. Hutmacher, Biodegradable polymers applied in tissue engineering research: a review, Polym. Int. 56 (2007) 145–157.
[8] S. Polizu, O. Savadogo, P. Poulin, L. Yahia, Applications of carbon nanotubes-based biomaterials in biomedical nanotechnology, J. Nanosci. Nanotechnol. 6 (2006) 1883–1904.
[9] K.S. Katti, Biomaterials in total joint replacement, Colloids Surf. B Biointerfaces 39 (2004) 133–142.
[10] S. Ramakrishna, J. Mayer, E. Wintermantel, K.W. Leong, Biomedical applications of polymer-composite materials: a review, Compos. Sci. Technol. 61 (2001) 1189–1224.
[11] R. Yoda, Elastomers for biomedical applications, J. Biomater. Sci. Polym. Ed. 9 (1998) 561–626.
[12] C. Gao, S. Peng, P. Feng, C. Shuai, Bone biomaterials and interactions with stem cells, Bone Res. 5 (2017) 17059.
[13] H.W. Ooi, S. Hafeez, C.A. van Blitterswijk, L. Moroni, M.B. Baker, Hydrogels that listen to cells: a review of cell-responsive strategies in biomaterial design for tissue regeneration, Mater. Horiz. 4 (2017) 1020–1040.
[14] S. Bersini, I.K. Yazdi, G. Talò, S.R. Shin, M. Moretti, A. Khademhosseini, Cell-microenvironment interactions and architectures in microvascular systems, Biotechnol. Adv. 34 (2016) 1113–1130.
[15] A.M. Hilderbrand, E.M. Ovadia, M.S. Rehmann, P.M. Kharkar, C. Guo, A.M. Kloxin, Biomaterials for 4D stem cell culture, Curr. Opin. Solid State Mater. Sci. 20 (2016) 212–224.
[16] M. Ahearne, Introduction to cell–hydrogel mechanosensing, Interface Focus 4 (2014) 20130038.
[17] X. Yao, R. Peng, J. Ding, Cell–material interactions revealed via material techniques of surface patterning, Adv. Mater. 25 (2013) 5257–5286.

[18] S. Martino, F. D'Angelo, I. Armentano, J.M. Kenny, A. Orlacchio, Stem cell-biomaterial interactions for regenerative medicine, Biotechnol. Adv. 30 (2012) 338–351.
[19] A. Seidi, M. Ramalingam, I. Elloumi-Hannachi, S. Ostrovidov, A. Khademhosseini, Gradient biomaterials for soft-to-hard interface tissue engineering, Acta Biomater. 7 (2011) 1441–1451.
[20] C.G. Simon, S. Lin-Gibson, Combinatorial and high-throughput screening of biomaterials, Adv. Mater. 23 (2011) 369–387.
[21] H. Shin, Fabrication methods of an engineered microenvironment for analysis of cell–biomaterial interactions, Biomaterials 28 (2007) 126–133.
[22] H. Shin, S. Jo, A.G. Mikos, Biomimetic materials for tissue engineering, Biomaterials 24 (2003) 4353–4364.
[23] L. Dao, C. Gonnermann, C.M. Franz, Investigating differential cell-matrix adhesion by directly comparative single-cell force spectroscopy, J. Mol. Recognit. 26 (2013) 578–589.
[24] C.M.P. Vidal, W. Zhu, S. Manohar, B. Aydin, T.A. Keiderling, P.B. Messersmith, A.K. Bedran-Russo, Collagen-collagen interactions mediated by plant-derived proanthocyanidins: a spectroscopic and atomic force microscopy study, Acta Biomater. 41 (2016) 110–118.
[25] P.N. Lewis, C. Pinali, R.D. Young, K.M. Meek, A.J. Quantock, C. Knupp, Structural interactions between collagen and proteoglycans are elucidated by three-dimensional electron tomography of bovine cornea, Structure 18 (2010) 239–245.
[26] A.L. Plant, K. Bhadriraju, T.A. Spurlin, J.T. Elliott, Cell response to matrix mechanics: focus on collagen, BBA-Mol. Cell Res. 1793 (2009) 893–902.
[27] M. Raspanti, T. Congiu, A. Alessandrini, P. Gobbi, A. Ruggeri, Different patterns of collagen-proteoglycan interaction: a scanning electron microscopy and atomic force microscopy study, Eur. J. Histochem. 44 (2000) 335–343.
[28] S. Perumal, O. Antipova, J.P.R.O. Orgel, Collagen fibril architecture, domain organization, and triple-helical conformation govern its proteolysis, Proc. Natl. Acad. Sci. U.S.A. 105 (2008) 2824–2829.
[29] G.W. Laurie, C.P. Leblond, G.R. Martin, Localization of type IV collagen, laminin, heparan sulfate proteoglycan, and fibronectin to the basal lamina of basement membranes, J. Cell Biol. 95 (1982) 340–344.
[30] M. Aumailley, N. Smyth, The role of laminins in basement membrane function, J. Anat. 193 (1998) 1–21.
[31] R. Sistiabudi, J. Paderi, A. Panitch, A. Ivanisevic, Modification of native collagen with cell-adhesive peptide to promote RPE cell attachment on Bruch's membrane, Biotechnol. Bioeng. 102 (2009) 1723–1729.
[32] J.C. Booij, D.C. Baas, J. Beisekeeva, T.G. Gorgels, A.A. Bergen, The dynamic nature of Bruch's membrane, Prog. Retin. Eye Res. 29 (2010) 1–18.
[33] A.E. Sorkio, E.P. Vuorimaa-Laukkanen, H.M. Hakola, H. Liang, T.A. Ujula, J.J. Valle-Delgado, M. Österberg, M.L. Yliperttula, H. Skottman, Biomimetic collagen I and IV double layer Langmuir–Schaefer films as microenvironment for human pluripotent stem cell derived retinal pigment epithelial cells, Biomaterials 51 (2015) 257–269.
[34] N. Lin, A. Dufresne, Nanocellulose in biomedicine: current status and future prospect, Eur. Polym. J. 59 (2014) 302–325.
[35] N. Halib, F. Perrone, M. Cemazar, B. Dapas, R. Farra, M. Abrami, G. Chiarappa, G. Forte, F. Zanconati, G. Pozzato, L. Murena, N. Fiotti, R. Lapasin, L. Cansolino, G. Grassi, M. Grassi, Potential applications of nanocellulose-containing materials in the biomedical field, Materials 10 (2017) 977.
[36] D. Klemm, F. Kramer, S. Moritz, T. Lindström, M. Ankerfors, D. Gray, A. Dorris, Nanocelluloses: a new family of nature-based materials, Angew. Chem. Int. Ed. 50 (2011) 5438–5466.
[37] M. Bhattacharya, M.M. Malinen, P. Lauren, Y.-R. Lou, S.W. Kuisma, L. Kanninen, M. Lille, A. Corlu, C. GuGuen-Guillouzo, O. Ikkala, A. Laukkanen, A. Urtti, M. Yliperttula, Nanofibrillar cellulose hydrogel promotes three-dimensional liver cell culture, J. Control. Release 164 (2012) 291–298.
[38] Y.-R. Lou, L. Kanninen, T. Kuisma, J. Niklander, L.A. Noon, D. Burks, A. Urtti, M. Yliperttula, The use of nanofibrillar cellulose hydrogel as a flexible three-dimensional model to culture human pluripotent stem cells, Stem Cells Dev. 23 (2014) 380–392.
[39] M.M. Malinen, L.K. Kanninen, A. Corlu, H.M. Isoniemi, Y.-R. Lou, M.L. Yliperttula, A.O. Urtti, Differentiation of liver progenitor cell line to functional organotypic cultures in 3D nanofibrillar cellulose and hyaluronan-gelatin hydrogels, Biomaterials 35 (2014) 5110–5121.
[40] D. Alsteens, H.E. Gaub, R. Newton, M. Pfreundschuh, C. Gerber, D.J. Müller, Atomic force microscopy-based characterization and design of biointerfaces, Nat. Rev. Mater. 2 (2017) 17008.
[41] W.A. Ducker, T.J. Senden, R.M. Pashley, Direct measurement of colloidal forces using an atomic force microscope, Nature 353 (1991) 239–241.
[42] J. Ralston, I. Larson, M.W. Rutland, A.A. Feiler, M. Kleijn, Atomic force microscopy and direct surface force measurements, Pure Appl. Chem. 77 (2005) 2149–2170.
[43] A. Carambassis, M.W. Rutland, Interactions of cellulose surfaces: effect of electrolyte, Langmuir 15 (1999) 5584–5590.
[44] J. Stiernstedt, N. Nordgren, L. Wågberg, H. Brumer, D.G. Gray, M.W. Rutland, Friction and forces between cellulose model surfaces: a comparison, J. Colloid Interface Sci. 303 (2006) 117–123.
[45] S. Ahola, J. Salmi, L.-S. Johansson, J. Laine, M. Österberg, Model films from native cellulose nanofibrils. Preparation, swelling, and surface interactions, Biomacromolecules 9 (2008) 1273–1282.
[46] M. Österberg, J.J. Valle-Delgado, Surface forces in lignocellulosic systems, Curr. Opin. Colloid Interface Sci. 27 (2017) 33–42.
[47] A.J.J. Goffin, J. Rajadas, G.G. Fuller, Interfacial flow processing of collagen, Langmuir 26 (2010) 3514–3521.
[48] J.J. Valle-Delgado, L.-S. Johansson, M. Österberg, Bioinspired lubricating films of cellulose nanofibrils and hyaluronic acid, Colloids Surf. B Biointerfaces 138 (2016) 86–93.
[49] J.E. Sader, J.W.M. Chon, P. Mulvaney, Calibration of rectangular atomic force microscope cantilevers, Rev. Sci. Instrum. 70 (1999) 3967–3969.
[50] H.-J. Butt, B. Cappella, B.M. Kappl, Force measurements with the atomic force microscope: technique, interpretation and applications, Surf. Sci. Rep. 59 (2005) 1–152.
[51] B. Derjaguin, L. Landau, Theory of the stability of strongly charged lyophobic sols and of the adhesion of strongly charged particles in solution of electrolytes, Acta Physicochim. URSS 14 (1941) 633–662.
[52] E.J.W. Verwey, J.T.G. Overbeek, Theory of the Stability of Lyophobic Colloids, Elsevier, Amsterdam, 1948.
[53] J.N. Israelachvili, Intermolecular and Surface Forces, third edition, Elsevier, London, 2011.
[54] W.R. Bowen, N. Hilal, R.W. Lovitt, C.J. Wright, Direct measurement of interactions between adsorbed protein layers using an atomic force microscope, J. Colloid Interface Sci. 197 (1998) 348–352.
[55] L. Bergström, S. Stemme, T. Dahlfors, H. Arwin, L. Ödberg, Spectroscopic ellipsometry characterisation and estimation of the Hamaker constant of cellulose, Cellulose 6 (1999) 1–13.
[56] P.D. Yurchenco, Y.S. Cheng, H. Colognato, Laminin forms an independent network in basement membranes, J. Cell Biol. 117 (1992) 1119–1133.
[57] U. Odenthal, S. Haehn, P. Tunggal, B. Merkl, D. Schomburg, C. Frie, M. Paulsson, N. Smyth, Molecular analysis of laminin N-terminal domains mediating self-interactions, J. Biol. Chem. 279 (2004) 44504–44512.
[58] K.K. McKee, D. Harrison, S. Capizzi, P.D. Yurchenco, Role of laminin terminal globular domains in basement membrane assembly, J. Biol. Chem. 282 (2007) 21437–21447.
[59] P. Eronen, K. Junka, J. Laine, M. Österberg, Interactions between water-soluble polysaccharides and native nanofibrillar cellulose thin films, Bioresources 6 (2011) 4200–4217.
[60] R. Timpl, H. Wiedemann, V. van Delden, H. Furthmayr, K. Kühn, A network model for the organization of type IV collagen molecules in basement membranes, Eur. J. Biochem. 120 (1981) 203–211.
[61] E.C. Tsilibary, A.S. Charonis, The role of the main noncollagenous domain (NC1) in type IV collagen self-assembly, J. Cell Biol. 103 (1986) 2467–2473.
[62] J.S. Graham, A.N. Vomund, C.L. Phillips, M. Grandbois, Structural changes in human type I collagen fibrils investigated by force spectroscopy, Exp. Cell Res. 299 (2004) 335–342.
[63] L. Bozec, M. Horton, Topography and mechanical properties of single molecules of type I collagen using atomic force microscopy, Biophys. J. 88 (2005) 4223–4231.
[64] A.S. Charonis, E.C. Tsilibary, P.D. Yurchenco, H. Furthmayr, Binding of laminin to type IV collagen: a morphological study, J. Cell Biol. 100 (1985) 1848–1853.
[65] D.T. Woodley, C.N. Rao, J.R. Hassell, L.A. Liotta, G.R. Martin, H.K. Kleinman, Interactions of basement membrane components, Biochim. Biophys. Acta 761 (1983) 278–283.